Bringing to light transient molecular structure and function using advanced vibrational spectroscopy

Strudwick, B.H.

Publication date
2019

Document Version
Other version

License
Other

CHAPTER 1

Introduction

1.1 New Light on Complex Molecules

The development of new chemical synthetic methods over the past century has made it possible to synthesise and construct complex compounds with specific tailor-made functionalities, such as photochromic molecular switches[1–5], molecular machines[6–9] and rotors[10–14] and self-assembled chiral supramolecules.[15–20] For many of these compounds, the functionality is a result of perturbing their electronic structure. Spectroscopists are therefore not only interested in resolving the absolute configuration and conformation of these molecules in the electronic ground state but also their dynamics in excited states. Observing such mechanisms can be experimentally difficult to achieve. For instance spectroscopic techniques such X-ray reflectometry,[7,20] electronic circular dichroism,[21–23] UV/vis transient-absorption spectroscopy,[5,6,24,25] cyclic voltammetry[4,26–28] and NMR[4,5,29] have all been used before with some success, but these methods often lack the time resolution to observe molecular dynamics (which typically occurs on a picosecond time scale[2,5,6,24,25,30]), spectral resolution to fully capture the intermediate species in a dynamic process or absolute configuration of chiral compounds; or more simply are unable to measure them in their working environment.

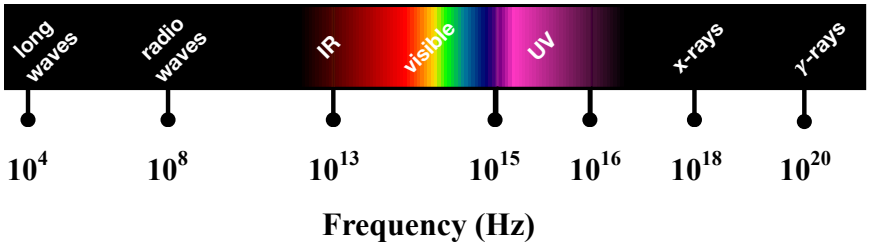

Figure 1.1: The electromagnetic spectrum. The infrared spectrum resides at lower frequencies than the visible spectrum and its spectral range is from near-infrared ($\lambda \sim 1$ µm) to far-infrared ($\lambda \sim 100$ µm).

Probing the vibrational modes of molecular systems resolves many of the challenges and limitations the aforementioned spectroscopic methods confront. Molecular vibrations are the periodic motions of the atoms in a molecule. The vibrations typically resonate in the infrared frequency (IR) region, see Figure 1.1. There are many benefits to using vibrational modes to investigate molecular structure, because some modes are specific to functional groups and can therefore act as local structural probes and provide information about the local environment.[31] The frequencies and intensities of vibrational absorption bands critically depend on the electronic structure of the molecule and can thus be used to trace the electronic evolution of the molecule, but they also provide a fingerprint of the molecular structure, thereby allowing the dynamics of the molecule to be followed in real time.[4,5] In the present thesis two advanced vibrational spectroscopic techniques, vibrational circular dichroism (VCD) and time-resolved vibrational spectroscopy (TRVS), are utilised to investigate a range of complex molecules and the dy-

namic processes that occur in these molecules upon activating them for specific purposes. VCD, which will be discussed in Section 1.3, is able to unambiguously identify the absolute configuration and the conformation of chiral compounds.[32–36] TRVS, discussed in Section 1.4, is able to observe processes on the picosecond timescale.[5,9,37,38]

1.2 Spectroscopy and Molecular Processes

Before discussing these two spectroscopic techniques a brief description of spectroscopy, which hinges on the interaction of molecules with electromagnetic radiation and molecular processes, will be discussed. One of the key observables to characterise this interaction experimentally is the absorbance (Abs), which is derived from the intensity difference between the incoming light (I_0) before passing through the sample and the transmitted light after it has interacted with the sample (I) and is given by Beer-Lambert's law:[39]

$$\text{Abs} = -\log_{10}(\frac{I}{I_0}) = \epsilon(\nu) \cdot l \cdot C, \tag{1.1}$$

where l is the path length over which the light interacts with the sample, C the concentration of the sample and $\epsilon(\nu)$ the wavelength-dependent molar absorptivity coefficient. Equation 1.1 can be understood quantum-mechanically by the relationship:[40]

$$A = \int \epsilon(\nu) d\nu = \frac{h\nu_{fi}}{c} N_A B_{if}, \tag{1.2}$$

where A is the integrated absorption coefficient, N_A Avogadro's number, c the speed of light, h is Planck's constant, ν_{fi} the frequency of the transition and B_{if} Einstein's coefficient for stimulated absorption. The transition rate from an initial state $|i\rangle$ to another state $|f\rangle$ is proportional to Einstein's coefficient of stimulated absorption following the relation:[41]

$$T_{i\to f} = B_{if}\rho(\Delta E_{fi}), \tag{1.3}$$

where $\rho(\Delta E_{fi})$ is the density of final states ($|f\rangle$) per unit of energy difference between the initial and excited state, ΔE_{fi}. The transition rate ($T_{i\to f}$) going from an initial state ($|i\rangle$) to another state ($|f\rangle$) is given by Fermi's Golden rule:[40,42,43]

$$T_{i\to f} = \frac{2\pi}{\hbar}|\langle f|H'|i\rangle|^2 \rho(\Delta E_{fi}) \tag{1.4}$$

$$H' = \boldsymbol{E} \cdot \boldsymbol{\mu}, \tag{1.5}$$

where H' is the perturbing Hamiltonian, $\boldsymbol{E}$ the electric field of the electromagnetic radiation and $\boldsymbol{\mu}$ the transition-dipole moment. Equation 1.5 shows that in order for a transition to occur the incoming photons must have a frequency and polarisation that match the frequency and direction of the oscillation of the transition

dipole moment.[44] Combining these expressions shows that absorption is due to a transition that promotes the system being perturbed from one state to another. In the present thesis the transitions of interest are transitions between different electronic states (electronic transitions) that typically occur in the UV/vis part of the electromagnetic spectrum and transitions between different vibrational states (vibrational transitions) that occur in the near- to far-infrared regions of the spectrum.

1.2.1 Theory of vibrational spectroscopy

This thesis is primarily concerned with utilising the vibrational modes of molecules to investigate their structure and behaviour. The simplest quantum mechanical description of a molecular vibration starts from the classical approach by considering a two-body system with masses m_1 and m_2 (the atoms) connected by a spring acting as the chemical bond, as depicted in Figure 1.2. The spring follows Hooke's law which contains a force constant k, and r the distance between the two atoms (r_e being the equilibrium bond length); classically this leads to simple harmonic motion with the potential energy of this system given by:[45]

$$V(x) = \frac{1}{2}kx^2, \tag{1.6}$$

where $x = r - r_e$ is the displacement from the equilibrium bond length. This gives a quadratic potential energy surface labelled "Harmonic" in Figure 1.2. The Hamiltonian of a quantum harmonic oscillator, the quantum-mechanical analog of simple harmonic motion, is given by the following expression:[46]

$$\hat{H} = -\frac{\hbar^2}{2\mu}\frac{d^2}{dr^2} + V(x), \tag{1.7}$$

where μ is the reduced mass of the system ($\mu = m_1 m_2 / m_1 + m_2$). Substituting Equation 1.6, into Equation 1.7 and rearranging the Schrödinger equation produces:[45,46]

$$\frac{d^2\Psi_n(x)}{dx^2} = -\frac{2\mu}{\hbar^2}(E_n - \frac{1}{2}kx^2)\Psi_n(x), \tag{1.8}$$

where $\Psi_n(x)$ and E_n is the wavefunction and energy of the system, respectively, for a given state n. Solving the Schrödinger equation gives the energy of the vibrational states:[45,46]

$$E_n = \hbar\omega(n + \frac{1}{2}), \tag{1.9}$$

where $n = 0, 1, 2, ...$ and ω ($\omega = \sqrt{k/\mu}$) the frequency of the vibrational mode. Equation 1.9 shows that the ground-state energy ($n = 0$), also known as the Zero Point Vibrational energy, is not zero but given by: $E_0 = \frac{1}{2}\hbar\omega$.[46] Transitions can occur between levels for which $n_f - n_i = \pm 1$ and are thus associated with an energy difference of $E_{fi} = \hbar\omega$. Whilst the quantum harmonic oscillator is a

good approximation for the lower energy levels, it fails for the higher ones. The Morse potential, shown in Figure 1.2, on the other hand includes the effect of anharmonicity due to bond dissociation occurring at large r, and is given by:[47]

$$V(x)_{Morse} = D_e(1 - e^{-ax})^2, \tag{1.10}$$

where D_e is the bond-dissociation energy and $a = \sqrt{k/D_e}$. Substituting Equation 1.10 into the Hamiltonian (Equation 1.7) and solving the Schrödinger equation results in the following expression for the energy of each vibrational state:[47]

$$E_n = \hbar\omega(n + \frac{1}{2}) - x(n + \frac{1}{2})^2, \tag{1.11}$$

For lower vibrational states such as $n = 0$ the Morse potential thus acts similar to a quantum harmonic oscillator, but, as we go to higher vibrational states the Morse potential successfully captures the anharmonicity that is seen experimentally.[48]

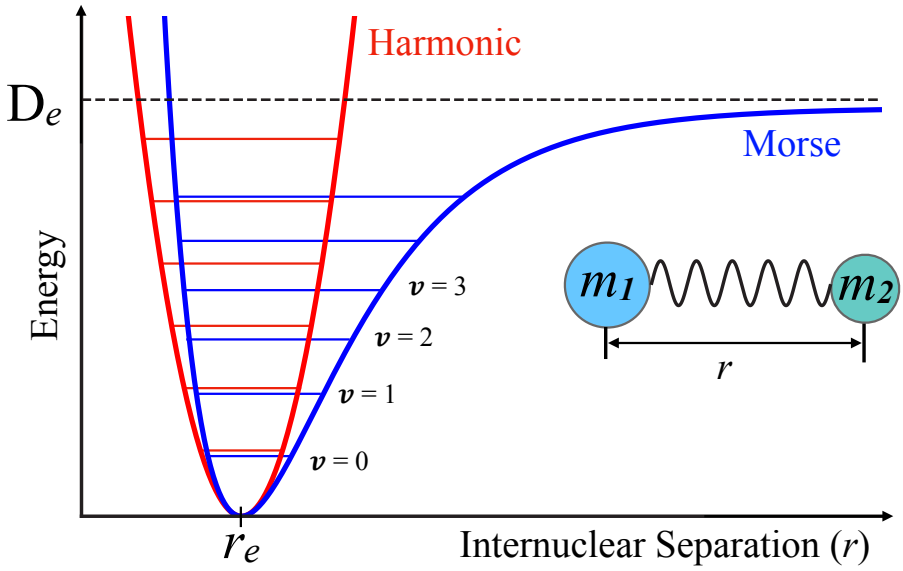

Figure 1.2: The potential well of a quantum harmonic oscillator (red) and the Morse potential well (blue) for a diatomic molecule.

1.2.2 Excited-State Molecular Processes

A Jablonski diagram[49] (Figure 1.3) illustrates the electronic states, transitions and molecular processes that can be found throughout this thesis. The absorption of a photon by a molecule can promote a molecule from the electronic ground state S_0 to a higher electronic state, S_1,S_2, ..., S_n . Eventually the molecule will relax to its ground state S_0, and in that process discard the excess energy, a process that can be achieved through multiple mechanisms. If the molecule is promoted to a state higher than its lowest-energy excited state, for example S_2 in Figure 1.3, then before returning to S_0 it can decay to S_1 by means of internal conversion, a non-radiative process in which the spin remains conserved.[50]

Since the potential energy curves of ground and electronically excited states are generally displaced with respect to each other, electronic excitation is often accompanied by vibrational excitation of the molecule in the electronic state that is excited, leading to a non-Bolzmann distribution of vibrational energy. Vibrational relaxation returns the population distribution to a Maxwell-Boltzmann distribution by a redistribution of the energy over accessible vibrational levels within the molecule and subsequently by transferring vibrational energy to the surrounding solvent molecules.

Fluorescence emission refers to the process in which the molecule emits a photon in order to discard the excess electronic energy. Photon emission can occur either by spontaneous emission[44] or stimulated emission[53]; a radiating transition dipole is established and the electron transitions from a energetically higher orbital, S_1 in Figure 1.3, to a lower-lying orbital (S_0). Another type of photon emission process, phosphorescence, may occur if the excited state undergoes intersystem crossing to an excited triplet state (T_1). This is formally a forbidden process[54] as it involves a change in spin, but becomes slightly allowed by spin-orbit coupling. This state can decay back to the ground state radiatively (phosphorescence) or via non-radiative internal conversion channels, explained below. Since both processes involve a forbidden change in spin, they occur on significantly longer time scales as the corresponding processes from the lowest excited singlet state (S_1).

Internal conversion to the ground state is generally a relatively slow process due to the large energy gap between the excited state and the ground state. However, in situations in which this energy gap is reduced the internal conversion rate will clearly increase. Conical intersections represent in this respect the most extreme form. They occur for molecular geometries where ground and excited state become degenerate.[55,56] Near such conical intersections electronic and nuclear motion are no longer decoupled, enabling an ultrafast relaxation from the excited state to the ground state.

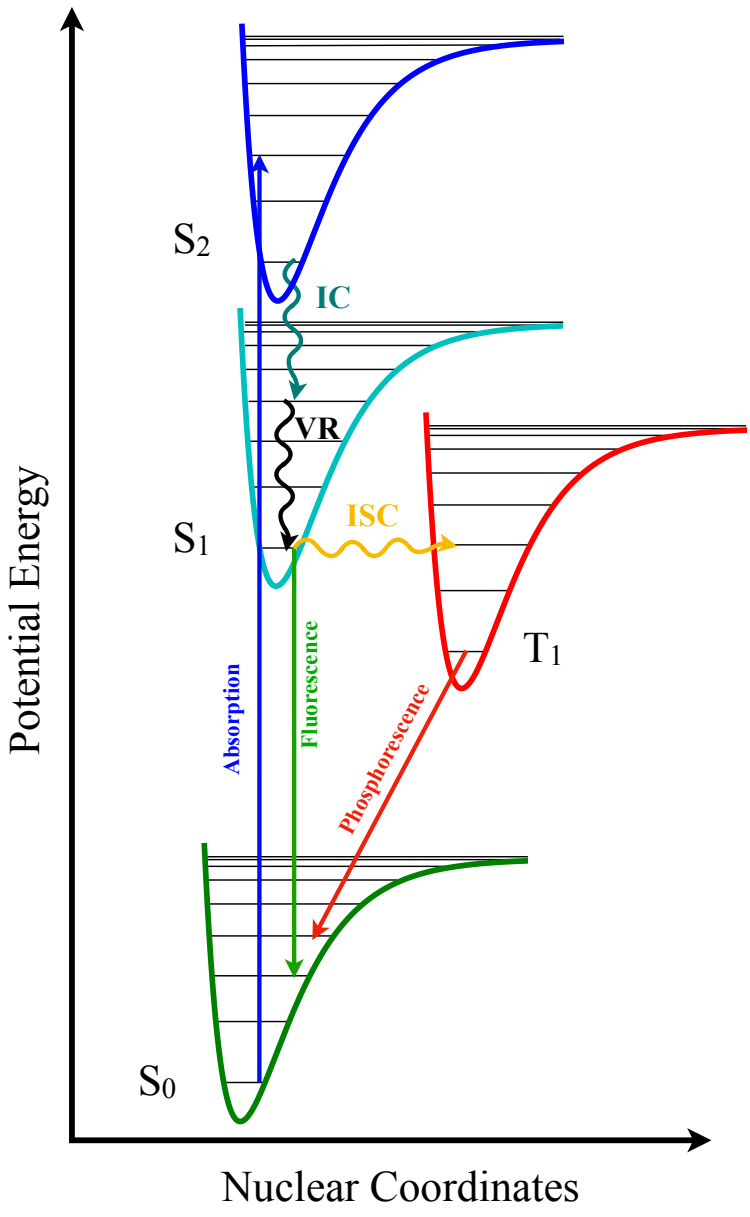

Figure 1.3: Jablonski Diagram: S_0, S_1 and S_2 are the electronic singlet states and T_1 is the electronic triplet state. IC: Internal Conversion, ISC: Intersystem Crossing and VR: Vibrational Relaxation; oscillating arrows represent non-radiative processes.

1.3 Vibrational Circular Dichroism

Optical activity, the property of rotating the plane of polarisation of plane-polarised light, was discovered in 1811 by François Jean Dominique Arago from the observation that light can pass through two crossed polarisers when a quartz crystal is placed between them.[57] Shortly after, in 1848, Louis Pasteur was working with tartaric acid (Figure 1.4) and demonstrated that naturally occurring tartaric acid exhibited optical activity while the synthetically produced form did not. He then noticed that the crystals from the synthetically produced tartaric acid came in two asymmetric forms that were optically active and the rotation of the polarisation were in opposite directions. The final brilliant step by Pasteur was to create an equimolar mix of the two forms which did not exhibit optical activity.[58,59] Finally, in 1874 Jacob Henricus van 't Hoff and Joseph Achille Le Bel proposed that optical activity is a result of the 3D asymmetrical structure carbon can produce when bonded to four different groups.[60,61] The 19th century provided us with the building blocks to establish chiral spectroscopy, and from it we know that enantiomers or optical isomers are non-superimposable mirror images whose optical activity are equal in magnitude but opposite in sign.[62] The nomenclature used within the chemistry/biology community for the optical isomers are S/L (left handed) and R/S (right handed).

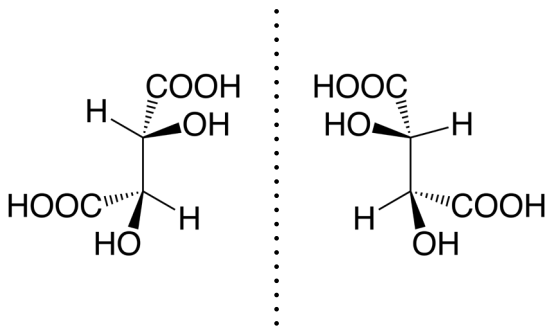

Figure 1.4: The two enantiomers of tartaric acid which Louis Pasteur separated and then observed their optical activity. Tartaric acid is in fact part of a group called meso compounds. It has two stereocenters. Shown to the left is the 2S,3S isomer and to the right the 2R,3R isomer which are optically active and opposite to one another. The 2R,3S and 2S,3R isomers, on the other hand, may have chiral centres but are superimposable and do not show optical activity.[63]

1.3.1 Circular Dichroism

Circular Dichroism is a chiroptical spectroscopic technique that measures the difference in absorption of left-circularly polarised (LCP) light and right-circularly polarised (RCP) light:[32–34]

$$\Delta A = A^L - A^R \tag{1.12}$$

where A^L and A^R are the absorption of LCP light and RCP light, respectively. Circularly polarised light (CPL) is composed of two plane waves of equal amplitude which are out of phase by $\pm\pi/2$. If the CPL is propagating along the z-axis then the electric and magnetic components can be expressed as:[40]

$$\boldsymbol{E}_{\pm}(t) = 2E_0(\cos(\Phi t)\boldsymbol{e}_x \pm \sin(\Phi t)\boldsymbol{e}_y) \tag{1.13}$$

$$\boldsymbol{B}_{\pm}(t) = 2B_0(\pm\sin(\Phi t)\boldsymbol{e}_x - \cos(\Phi t)\boldsymbol{e}_y) \tag{1.14}$$

where E_0 and B_0 are the time-independent amplitudes, $\boldsymbol{e}_{x/y}$ the unit vectors and $\Phi t = \omega(t - z/c)$. The $\pm$ label in Equations 1.13 and 1.14 assign the handedness of the CPL ("+" for LCP and "−" for RCP). A classical interpretation of circular dichroism is described in Figure 1.5.

Now consider a chiral compound irradiated by CPL. The transition probability will follow Fermi's Golden Rule (Equation 1.4). The perturbation Hamiltonian for this transition is dependent on the handedness of the phase shifted $\boldsymbol{E}_{\pm}$ and $\boldsymbol{B}_{\pm}$ vector components:

$$H' = -\boldsymbol{\mu}_{el} \cdot \boldsymbol{E}_{\pm} - \boldsymbol{\mu}_{mag} \cdot \boldsymbol{B}_{\pm} \tag{1.15}$$

where $\boldsymbol{\mu}_{el}$ and $\boldsymbol{\mu}_{mag}$ are the electric and magnetic transition-dipole operators. Substitution of Equations 1.13 and 1.14 into Equation 1.15 and then substituting the Hamiltonian into Equation 1.4, followed by some rearrangements, produces the transition rate depending on the handedness of the CPL:[40,64]

$$T^{\pm}_{i\to f} = \frac{2\pi}{3\hbar^2}[|\langle i|\boldsymbol{\mu}_{el}|f\rangle|^2 + |\langle f|\boldsymbol{\mu}_{mag}|i\rangle|^2 \pm 2i\langle i|\boldsymbol{\mu}_{el}|f\rangle \cdot \langle i|\boldsymbol{\mu}_{mag}|f\rangle]\rho(\Delta E_{fi}) \tag{1.16}$$

where we use Einstein's transition probabilities and Equation 1.3 to get Einstein's coefficient of stimulated absorption for CPL ($B^{\pm}_{if}$):[41]

$$B^{\pm}_{if} = \frac{2\pi}{3\hbar^2}[|\langle i|\boldsymbol{\mu}_{el}|f\rangle|^2 + |\langle f|\boldsymbol{\mu}_{mag}|i\rangle|^2 \pm 2i\langle i|\boldsymbol{\mu}_{el}|f\rangle \cdot \langle f|\boldsymbol{\mu}_{mag}|i\rangle]. \tag{1.17}$$

The next step is to obtain the absorption for both left- and right-CPL in relation to Einstein's coefficient of absorption using Beer-Lambert's law and Equation 1.2 to produce the difference in absorption of the CPL:[39,40]

$$\Delta A = A^L - A^R = \frac{h\nu_{fi}}{c} N_A(B^+_{if} - B^-_{if}) \tag{1.18}$$

Finally, by substituting Equation 1.17 for each handedness into Equation 1.18 we get the following expressions:[33,34,36]

$$\Delta A = (\frac{32\pi^3}{3})(\frac{\nu_{fi}N_A}{hc})Im[\langle i|\boldsymbol{\mu}_{el}|f\rangle \cdot \langle f|\boldsymbol{\mu}_{mag}|i\rangle] \tag{1.19}$$

$$R_{if} = Im[\langle i|\boldsymbol{\mu}_{el}|f\rangle \cdot \langle f|\boldsymbol{\mu}_{mag}|i\rangle] \tag{1.20}$$

where R_{if} is defined as the rotational strength of the transition. R_{if} is a real quantity since $\boldsymbol{\mu}_{mag}$ is an imaginary operator and Equation 1.19 thus shows that the differential absorption signal (ΔA) is proportional to the rotational strength.

1.3.2 Putting the V into VCD

The rotational strength, R_{if} (Equation 1.20) gives us a general framework for the absorption of CPL by a chiral compound. However, the calculation of R_{if} is different depending on the type of transition (electronic or vibrational). Intuitively, one might expect that calculations of R_{if} for vibrational transitions would be relatively easy as we would solely be working with the electronic ground state, but difficulties arise when applying the Born-Oppenheimer (BO) approximation to calculate R_{if} within the electronic ground state. The BO approximation assumes that the motion of the electrons and the nuclei can be treated independently.[65] The wave function Ψ of the molecule can be split up into two components $\Psi = \psi\chi$ where ψ and χ are the electronic and nuclear wave functions, respectively. Furthermore, the electric and magnetic transition-dipole operators ($\boldsymbol{\mu}_{el}$ and $\boldsymbol{\mu}_{mag}$) in the Hamiltonian (Equation 1.15) can be split up into electronic and nuclear contributions ($\boldsymbol{\mu}_{el} = \boldsymbol{\mu}^e_{el} + \boldsymbol{\mu}^n_{el}$ and $\boldsymbol{\mu}_{mag} = \boldsymbol{\mu}^e_{mag} + \boldsymbol{\mu}^n_{mag}$). Introducing the BO approximation to calculate R_{if} (Equation 1.20) for a vibrational transition from $\nu \rightarrow \nu'$ of a non-degenerate electronic state K results in the following expressions for each component:

$$\langle \Psi_{K\nu}|\boldsymbol{\mu}_{el}|\Psi_{K\nu'}\rangle = \langle \chi_{K\nu}|\langle \psi_K|\boldsymbol{\mu}^e_{el}|\psi_K\rangle + \boldsymbol{\mu}^n_{el}|\chi_{K\nu'}\rangle \tag{1.21}$$

$$\langle \Psi_{K\nu}|\boldsymbol{\mu}_{mag}|\Psi_{K\nu'}\rangle = \langle \chi_{K\nu}|\langle \psi_K|\boldsymbol{\mu}^e_{mag}|\psi_K\rangle + \boldsymbol{\mu}^n_{mag}|\chi_{K\nu'}\rangle \tag{1.22}$$

However, the electronic magnetic transition-dipole moment $\boldsymbol{\mu}^e_{mag}$ acting on a single non-degenerate electronic state (ψ_K) yields zero due to the characteristic of the operator:[66]

$$\langle \psi_K|\boldsymbol{\mu}^e_{mag}|\psi_K\rangle = 0 \tag{1.23}$$

which would lead to the conclusion that only the nuclei contribute to the magnetic transition-dipole moment. To resolve this issue a description beyond the BO approximation is needed.[33,67] By utilising first-order perturbation theory on the BO wave functions (ψ and χ) and including the kinetic energy operator (T_N), that

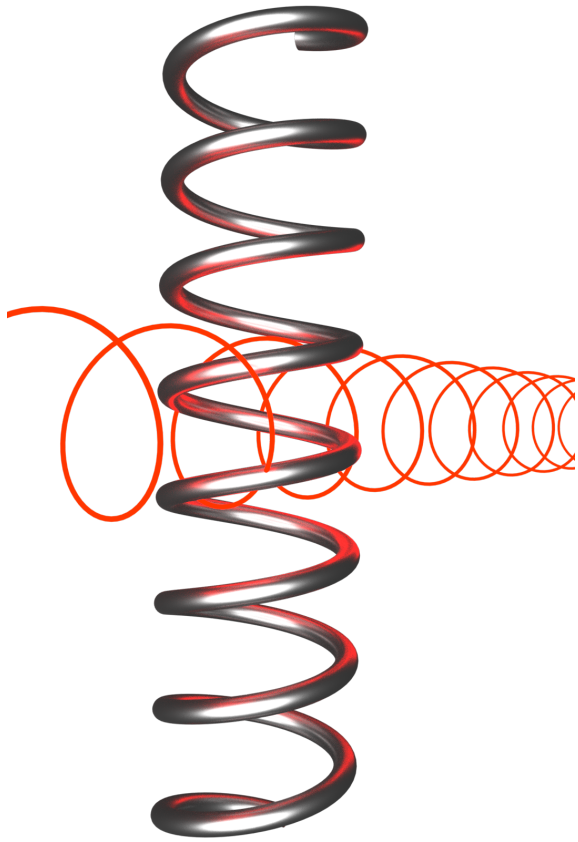

Figure 1.5: From a classical viewpoint chiral molecules can be considered as conducting coils. Aligned copper coils have shown strong optical activity when subjected to plane polarised microwave radiation whose incidence is orthogonal to the helical axis of the spring.[73] Depicted here is a conducting coil that is being perturbed by RCP light orthogonal to the helical axis. When CPL passes through the coil both the electric field and the magnetic field exert a force on the electrons in the wire; the change of the magnetic flux over time through the wire leads to an electromotive force.[74] Depending on the handedness of the helicity of the coil the electromotive force will work in the same or opposite direction of the electrical force. This results in a difference in the current produced for LCP light and RCP light, and therefore there is difference in the amount of LCP light absorbed compared with RCP light producing a ΔA (Equation 1.12).

is neglected under the BO approximation, one can obtain an electronic contribution to the magnetic transition-dipole moment and therefore a contribution to the rotational strength which is given by:[33,68]

$$\langle\Psi|\boldsymbol{\mu}^{e}_{mag}|\Psi\rangle = \left\langle \chi_{0\nu} \middle| \sum_{K\neq 0} \frac{\langle\psi_0|\boldsymbol{\mu}^{e}_{mag}|\psi_n\rangle}{E_K - E_0}(\langle\psi_K|T_N|\psi_0\rangle - \langle\psi_0|T_N|\psi_K\rangle) \middle| \chi_{0\nu'} \right\rangle \tag{1.24}$$

where E_0 and E_n are the electronic ground state ($K = 0$) and the K^{th} electronic state energies, respectively. This shows that the VCD signal intensities are proportional to the sum of the magnetic transition-dipole moments weighted by the electronic transition energies ($E_K - E_0$). This explains the small VCD signal sizes seen for organic compounds, because they tend to have large differences in energy between their electronic ground state ($K = 0$), and their first excited electronic state ($K = 1$). For this reason, VCD signals are typically 10^{-4}– 10^{-5} times smaller than their corresponding IR signals. However, it has been shown experimentally in the past and will be used in the present thesis, that VCD signal intensities can be dramatically increased by manipulating the electronic manifold in a way that reduces the energy differences: $E_K - E_0$.[69–72]

1.4 Time-resolved Vibrational Spectroscopy

Time-resolved spectroscopy studies the dynamic processes of biological, chemical or physical systems and can be applied to capture the changes to the absorption and emission of a system.[8,9,56,75,76] Early work in the 1940s and 1950s investigated reaction kinetics on a millisecond to a microsecond time scale.[77,78]. In this thesis we are concerned with a type of time-resolved spectroscopy known as pump-probe spectroscopy (see subsection 1.4.1). For the molecular processes that we want to observe directly in the time domain, one needs lasers that produce pulses with a duration in the order of tens to hundreds of femtoseconds. The first major breakthroughs were in 1960 and 1963 with the development of the laser[79] and the first demonstration of a mode-locked laser[80] which is essential for generating femtosecond pulses. Finally, in 1982 Peter F. Moulton developed the titanium-sapphire laser[81], the type of solid-state femtosecond pulsed lasers that is used throughout this thesis.

1.4.1 Pump-probe spectroscopy

Pump-probe spectroscopy uses two spectra, the absorption of the perturbed sample and of the unperturbed sample, to construct a transient spectrum (see Figure 1.6). The unperturbed spectrum is simply taken by observing the transmission spectrum with a probe pulse, and for TRVS mid-IR radiation is used to probe the vibrational modes. In order to obtain the perturbed spectrum a “pump” has to be introduced to the sample before the mid-IR probe pulse passes through the sample. The

transient absorption spectrum is produced by taking the difference of the two spectra (pumped and unpumped):

$$\Delta A_{ta} = A_p - A_u \tag{1.25}$$

where ΔA_{ta} is the transient absorption spectrum and A_p and A_u are the pumped and unpumped absorption spectra, respectively. In our case UV/visible radiation will be used to excite compounds into an electronic excited state, and as the frequencies and intensities of vibrational absorption bands in the mid-IR critically depend on the electronic structure of the molecule the result is that A_p and A_u spectra are generally significantly different. Figure 1.6 gives a schematic illustration of Equation 1.25. The blue spectrum shows the absorption spectrum of our unperturbed molecule (A_u) and for simplicity it only has one vibrational band with a frequency ω_g. When excited with a photon the molecule or sample will be promoted into an excited state where the electronic structure of the molecule has changed; this affects the vibrational mode and changes the frequency to ω_e producing a new absorption spectrum (A_p) shown in red. The transient absorption spectrum shown in green is constructed using Equation 1.25 and is equivalent to subtracting the blue spectrum from the red spectrum. This results in a spectrum that has both positive and negative absorption bands. The negative absorption bands are thus associated with the depletion of the population of molecules in their ground state (ground-state bleach) and the positive absorption bands are from molecules that have been promoted from the ground state into their excited state species. The ground-state bleach is the mirror image of the steady-state IR spectrum of the compound, and the transient absorption spectrum contains the features of the electronically excited molecule.

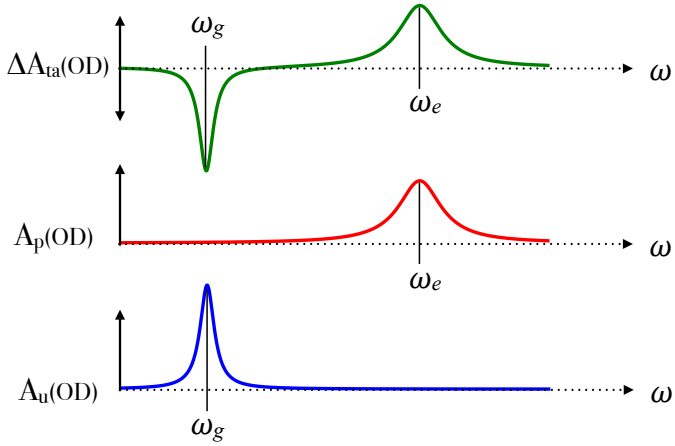

Figure 1.6: Top: transient absorption spectrum which is constructed from the measured pumped and unpumped spectra (Equation 1.25) of the sample. Middle: absorption spectrum of the sample in its excited perturbed state; Bottom: spectrum of the sample in its unperturbed ground state.

1.5 Outline and scope of the thesis

This thesis describes experimental and computational research using two distinct techniques: vibrational circular dichroism and transient absorption spectroscopy. In Chapter 2 the experimental methods and data analysis used in the thesis are discussed. It describes the techniques and spectrometers used to measure steady-state Infrared Absorption and Vibrational Circular Dichroism, and the spectro-electrochemical measurement methods. It also provides a description of nano- and femtosecond transient absorption setups as well as the femtosecond transient infrared absorption setups. In Chapter 3 a mechanistic study of a non-C_3-symmetric triethynyl terthiophene system is presented. Here we utilise UV/vis and infrared transient absorption spectroscopy combined with quantum chemical studies (DFT) to understand the ultrafast dynamics of the system. In Chapter 4 time-resolved vibrational spectroscopy studies are reported on the photoinduced structural dynamics of 2,2-diphenyl-2H-chromene. These types of photochromic molecules are used in various applications ranging from self-coloring sun glasses to advanced electrooptical technologies. Nevertheless, there is still a large debate on the structural evolution processes that occur upon light absorption. Here, tansient IR absorption measurements in combination with (TD)-DFT calculations are used to unveil the key details of the life cycle of such compounds. Chapter 5 describes studies on a fluorescent meso-substituted boron-dipyrromethene (BODIPY) molecular rotor. Fluorescence quantum yields and time-resolved vibrational spectroscopic measurements of the molecular rotor are reported for various different solvents. The comparison between the two techniques enables us to understand the excited-state dynamics of BODIPY and the effect of the solvent on the excited state species. Chapter 6 reports VCD measurements on a achiral homogeneous rhodium-based hydrogenation catalyst that becomes enantioselective when a chiral cofactor binds non-covalently to the bisphosphine ligand. The experimentally obtained VCD spectra in combination with DFT calculations are used to investigate the structure of the entire catalytic complex, and to investigate whether these spectra might be used to predict the observed enantioselectivity. In Chapter 7, vibrational circular dichroism (VCD) studies are reported on a prototypical chiral compound that has multiple redox states. VCD and UV/vis spectroelectrochemical measurements in combination with (TD-)DFT calculations have been used to investigate how the spatial extent of a molecular moiety (in this case C_{60}) , whose electronic excitation energies can be modulated electrochemically, affects its performance as a molecular amplifier for VCD signals.

References

1. Jayasuriya, N.; Kagan, J.; Owens, J. E.; Kornak, E. P.; Perrine, D. M. Photocyclization of terthiophenes. *J. Org. Chem.* **1989**, *54*, 4203–4205.
2. Herzog, T. T.; Ryseck, G.; Ploetz, E.; Cordes, T. The photochemical ring opening reaction of chromene as seen by transient absorption and fluorescence spectroscopy. *Photochem. Photobiol. Sci.* **2013**, *12*, 1202–1209.
3. Irie, M.; Fukaminato, T.; Matsuda, K.; Kobatake, S. Photochromism of diarylethene molecules and crystals: Memories, switches, and actuators. *Chem. Rev.* **2014**, *114*, 12174–12277.
4. Zhang, J.; Sun, C.-F.; Zhang, M.-X.; Hartl, F.; Yin, J.; Yu, G.-A.; Rao, L.; Liu, S. H. Asymmetric oxidation of vinyl- and ethynyl terthiophene ligands in triruthenium complexes. *Dalton Trans.* **2016**, *45*, 768–782.
5. Strudwick, B. H.; Zhang, J.; Hilbers, M. F.; Buma, W. J.; Woutersen, S.; Liu, S. H.; Hartl, F. Excited-State Electronic Asymmetry Prevents Photoswitching in Terthiophene Compounds. *Inorg. Chem.* **2018**, *57*, 9039–9047.
6. Brouwer, A. M.; Frochot, C.; Gatti, F. G.; Leigh, D. A.; Mottier, L.; Paolucci, F.; Roffia, S.; Wurpel, G. W. H. Photoinduction of Fast, Reversible Translational Motion in a Hydrogen-Bonded Molecular Shuttle. *Science* **2001**, *291*, 2124–2128.
7. Nørgaard, K.; Laursen, B. W.; Nygaard, S.; Kjaer, K.; Tseng, H.-R.; Flood, A. H.; Stoddart, J. F.; Bjørnholm, T. Structural Evidence of Mechanical Shuttling in Condensed Monolayers of Bistable Rotaxane Molecules. *Angew. Chem. Int. Ed.* **2005**, *44*, 7035–7039.
8. Panman, M. R.; Bodis, P.; Shaw, D. J.; Bakker, B. H.; Newton, A. C.; Kay, E. R.; Brouwer, A. M.; Buma, W. J.; Leigh, D. A.; Woutersen, S. Operation Mechanism of a Molecular Machine Revealed Using Time- Resolved Vibrational Spectroscopy. *Science* **2010**, *328*, 1255–1258.
9. Panman, M. R.; Bodis, P.; Shaw, D. J.; Bakker, B. H.; Newton, A. C.; Kay, E. R.; Leigh, D. A.; Buma, W. J.; Brouwer, A. M.; Woutersen, S. Time-resolved vibrational spectroscopy of a molecular shuttle. *Phys. Chem. Chem. Phys.* **2012**, *14*, 1865–1875.
10. Kuimova, M. K.; Yahioglu, G.; Levitt, J. A.; Suhling, K. Molecular Rotor Measures Viscosity of Live Cells via Fluorescence Lifetime Imaging. *J. Am. Chem. Soc.* **2008**, *130*, 6672–6673.
11. Levitt, J. A.; Kuimova, M. K.; Yahioglu, G.; Chung, P.-H.; Suhling, K.; Phillips, D. Membrane-Bound Molecular Rotors Measure Viscosity in Live Cells via Fluorescence Lifetime Imaging. *J. Phys. Chem. C* **2009**, *113*, 11634–11642.
12. Levitt, J. A.; Chung, P. H.; Kuimova, M. K.; Yahioglu, G.; Wang, Y.; Qu, J.; Suhling, K. Fluorescence anisotropy of molecular rotors. *ChemPhysChem* **2011**, *12*, 662–672.
13. Suhina, T.; Amirjalayer, S.; Woutersen, S.; Bonn, D.; Brouwer, A. M. Ultrafast

dynamics and solvent-dependent deactivation kinetics of BODIPY molecular rotors. *Phys. Chem. Chem. Phys.* **2017**, *19*, 19998–20007.

14. Hughes, A. R.; Brownbill, N. J.; Lalek, R. C.; Briggs, M. E.; Slater, A. G.; Cooper, A. I.; Blanc, F. Ultra-Fast Molecular Rotors within Porous Organic Cages. *Chem. Eur. J* **2017**, *23*, 17217–17221.
15. Zarges, W.; Hall, J.; Lehn, J. M. M.; Bolm, C. Helicity Induction in Helicate Self-Organisation from Chiral Tris(bipyridine) Ligand Strands. *Helv. Chim. Acta.* **1991**, *74*, 1843–1852.
16. Ghadiri, M. R.; Granja, J. R.; Milligan, R. A.; McRee, D. E.; Khazanovich, N. Self-assembling organic nanotubes based on a cyclic peptide architecture. *Nature* **1993**, *366*, 324–327.
17. Conn, M. M.; Rebek Jr., J. Self-Assembling Capsules. *Chem. Rev.* **1997**, *97*, 1647–1668.
18. Prins, L. J.; Huskens, J.; De Jong, F.; Timmerman, P.; Reinhoudt, D. N. Complete asymmetric induction of supramolecular chirality in a hydrogen-bonded assembly. *Nature* **1999**, *398*, 498–502.
19. Hirschberg, J. H. K. K.; Brunsveid, L.; Ramzi, A.; Vekemans, J.; Sijbesma, R.; Meijer, E. W. Helical self-assembled polymers from cooperative stacking of hydrogen-bonded pairs. *Nature* **2000**, *407*, 167–170.
20. Dydio, P.; Rubay, C.; Gadzikwa, T.; Lutz, M.; H Reek, J. N. " Cofactor " -Controlled Enantioselective Catalysis. *J. Am. Chem. Soc* **2011**, *133*, 17176–17179.
21. Koumura, N.; Zijlstra, R. W. J.; van Delden, R. A.; Harada, N.; Feringa, B. L. Light-driven monodirectional molecular rotor. *Nature* **1999**, *401*, 152 EP –.
22. Mendicuti, F.; González-Álvarez, M. J. Supramolecular chemistry: Induced circular dichroism to study host-guest geometry. *J. Chem. Educ.* **2010**, *87*, 965–968.
23. Panda, M.; Walmsley, J. A. Circular dichroism study of supramolecular assemblies of guanosine 5'-monophosphate. *J. Phys. Chem. B* **2011**, *115*, 6377–6383.
24. Gentili, P. L.; Danilov, E.; Ortica, F.; Rodgers, M. A. J.; Favaro, G. Dynamics of the excited states of chromenes studied by fast and ultrafast spectroscopies. *Photochem. Photobiol. Sci.* **2004**, *3*, 886–891.
25. Moine, B.; Réhault, J.; Aloïse, S.; Micheau, J. C.; Moustrou, C.; Samat, A.; Poizat, O.; Buntinx, G. Transient absorption studies of the photochromic behavior of 3H-naphtho[2,1-b]pyrans linked to thiophene oligomers via an acetylenic junction. *J. Phys. Chem. A* **2008**, *112*, 4719–4726.
26. Zhu, S. S.; Carroll, P. J.; Swager, T. M. Conducting polymetallorotaxanes: A supramolecular approach to transition metal ion sensors. *J. Am. Chem. Soc.* **1996**, *118*, 8713–8714.
27. Badji, J. D.; Balzani, V.; Credi, A.; Silvi, S.; Stoddart, J. F. A Molecular Elevator. *Science* **2004**, *303*, 1845–1849.
28. Vignon, S. A.; Jarrosson, T.; Iijima, T.; Tseng, H. R.; Sanders, J. K.; Stod-

dart, J. F. Switchable neutral bistable rotaxanes. *J. Am. Chem. Soc.* **2004**, *126*, 9884–9885.

29. Gatti, F. G.; Leon, S.; Wong, J. K. Y.; Bottari, G.; Altieri, A.; Morales, M. A. F.; Teat, S. J.; Frochot, C.; Leigh, D. A.; Brouwer, A. M.; Zerbetto, F. Photoisomerization of a rotaxane hydrogen bonding template: Light-induced acceleration of a large amplitude rotational motion. *Proc. Natl. Acad. Sci. U.S.A.* **2003**, *100*, 10–14.
30. Horng, M. L.; Gardecki, J. A.; Maroncelli, M. Rotational dynamics of coumarin 153: Time-dependent friction, dielectric friction, and other nonhydrodynamic effects. *J. Phys. Chem. A* **1997**, *101*, 1030–1047.
31. Ganim, Z.; Hoi, S. C.; Smith, A. W.; Deflores, L. P.; Jones, K. C.; Tokmakoff, A. Amide I two-dimensional infrared spectroscopy of proteins. *Acc. Chem. Res.* **2008**, *41*, 432–441.
32. Snatzke, G. Circular Dichroism and Absolute Conformation: Application of Qualitative MO Theory to Chiroptical Phenomena. *Angew. Chem. Int. Ed. Engl.* **1979**, *18*, 363–377.
33. Stephens, P. J. Theory of Vibrational Circular Dichroism. *J. Phys. Chem.* **1985**, *89*, 748–752.
34. Nafie, L. A. *Vibrational Optical Activity*; John Wiley & Sons, Ltd: Chichester, UK, 2011.
35. Merten, C.; Smyrniotopoulos, V.; Tasdemir, D. Assignment of absolute configurations of highly flexible linear diterpenes from the brown alga *Bifurcaria bifurcata* by VCD spectroscopy. *Chem. Commun.* **2015**, *51*, 16217–16220.
36. Merten, C. Vibrational optical activity as probe for intermolecular interactions. *Phys. Chem. Chem. Phys.* **2017**, *19*, 18803–18812.
37. Khalil, M.; Demirdöven, N.; Tokmakoff, A. Coherent 2D IR spectroscopy: Molecular structure and dynamics in solution. *J. Phys. Chem. A* **2003**, *107*, 5258–5279.
38. Rezus, Y. L. A.; Bakker, H. J. Orientational dynamics of isotopically diluted H_2O and D_2O. *J. Chem. Phys.* **2006**, *125*, 144512.
39. Swinehart, D. F. The Beer-Lambert Law. *J. Chem. Educ.* **1962**, *39*, 333.
40. Atkins, P. W.; Friedman, R. S. *Molecular Spectroscopy*; Oxford University Press, 2005.
41. Hilborn, R. C. Einstein coefficients, cross sections, f values, dipole moments, and all that. *Am. J. Phys.* **1982**, *50*, 982–986.
42. Levine, I. N. *Molecular Spectroscop* ; John Wiley & Sons, Ltd: New York, London, Sydney, Toronto, 1975.
43. Fermi, E. Versuch einer Theorie der beta-Strahlen. I. *Z. Physik* **1934**, *88*, 161–177.
44. Atkins, P. W.; Friedman, R. S. *Molecular quantum mechanics*; Oxford University Press, 2011.
45. Steele, D. *Theory of vibrational spectroscopy*; Philadelphia: Saunders, 1971.

46. Griffiths, D. J. *Introduction to quantum mechanics*; Cambridge University Press, 2016.
47. Morse, P. M. Diatomic molecules according to the wave mechanics. II. vibrational levels. *Phys. Rev.* **1929**, *34*, 57–64.
48. Le Roy, R. J.; Dattani, N. S.; Coxon, J. A.; Ross, A. J.; Crozet, P.; Linton, C. Accurate analytic potentials for $Li_2(X^1\Sigma_g^+)$ and $Li_2(A^1\Sigma_u^+)$ from 2 to 90 Å, and the radiative lifetime of Li(2p). *J. Chem. Phys.* **2009**, *131*, 204309.
49. Jablonski, A. Efficiency of Anti-Stokes Fluorescence in Dyes. *Nature* **1933**, *131*, 839–840.
50. Bixon, M.; Jortner, J. Intramolecular Radiation Transitions. *J. Phys. Chem.* **1968**, *48*, 715–726.
51. Owrutsky, J. C.; Raftery, D.; Hochstrasser, R. M. Vibrational Relaxation Dynamics in Solutions. *Annu. Rev. Phys. Chem.* **1994**, *45*, 519–555.
52. Pearman, R.; Gruebele, M. On the importance of higher order anharmonic molecular couplings. *J. Phys. Chem.* **1998**, *108*, 6561–6570.
53. Scully, M. O.; Zubairy, M. S. *Quantum optics*; Cambridge University Press, 1999.
54. Bunker, P. R.; Jensen, P. *Molecular Symmetry and Spectroscopy, 2nd Ed.*; NRC Research Press, 2006.
55. Teller, E. The Crossing of Potential Surfaces. *J. Phys. Chem.* **1937**, *41*, 109–116.
56. Polli, D.; Altoè, P.; Weingart, O.; Spillane, K. M.; Manzoni, C.; Brida, D.; Tomasello, G.; Orlandi, G.; Kukura, P.; Mathies, R. A.; Garavelli, M.; Cerullo, G. Conical intersection dynamics of the primary photoisomerization event in vision. *Nature* **2010**, *467*, 440–443.
57. Arago, F. J. D. Mémoire sur une modification remarquable qu'éprouvent les rayons lumineux dans leur passage à travers certains corps diaphanes et sur quelques autres nouveaux phénomènes d'optique. *Mémoires de la classe des sciences mathématiques et physiques de l'Institut Impérial de France* **1811**, *1st part*, 93–134.
58. Pasteur, L. Mémoire sur la relation qui peut exister entre la forme cristalline et la composition chimique, et sur la cause de la polarisation rotatoire. *Comptes rendus de l'Académie des sciences (Paris)* **1848**, *26*, 535–538.
59. Pasteur, L. Sur les relations qui peuvent exister entre la forme cristalline, la composition chimique et le sens de la polarisation rotatoire. *Annales de Chimie et de Physique* **1848**, *24*, 442–459.
60. Van 't Hoff, J. H. Sur les formules de structure dans l'espace. *Archives Néerlandaises des Sciences Exactes et Naturelles* **1874**, *9*, 445–454.
61. Le Bel, J. A. Sur les relations qui existent entre les formules atomiques des corps organiques et le pouvoir rotatoire de leurs dissolutions. *Bulletin de la Société Chimique de Paris* **1874**, *22*, 337–347.
62. Thomson, W., Baron Kelvin *Baltimore Lectures on Molecular Dynamics and*

the Wave Theory of Light; Cambridge Library Collection - Physical Sciences; Cambridge University Press, 2010.

63. McMurry, J. *Organic Chemistry*; International student edition; Thomson Brooks/Cole, 2008.
64. Barron, L. D. *Molecular Light Scattering and Optical Activity*; Cambridge University Press, 2004.
65. Born, M.; Oppenheimer, J. R. Zur Quantentheorie der Molekeln. *Annalen der Physik* **1927**, *389*, 457–484.
66. Faulkner, T. R.; Marcott, C.; Moscowitz, A.; Overend, J. Anharmonic effects in vibrational circular dichroism. *J. Am. Chem. Soc.* **1977**, *99*, 8160–8168.
67. Nafie, L. A.; Freedman, T. B. Vibronic coupling theory of infrared vibrational transitions. *J. Chem. Phys.* **1983**, *78*, 7108–7116.
68. Schrödinger, E. Quantisierung als Eigenwertproblem. *Annalen der Physik* **1926**, *80*, 437–490.
69. Domingos, S. R.; Panman, M. R.; Bakker, B. H.; Hartl, F.; Buma, W. J.; Woutersen, S. Amplifying vibrational circular dichroism by manipulation of the electronic manifold. *Chem. Commun.* **2012**, *48*, 353–355.
70. Domingos, S. R.; Sanders, H. J.; Hartl, F.; Buma, W. J.; Woutersen, S. Switchable amplification of vibrational circular dichroism as a probe of local chiral structure. *Angew. Chem. Int. Ed.* **2014**, *53*, 14042–5.
71. Domingos, S. R.; Huerta-Viga, A.; Baij, L.; Amirjalayer, S.; Dunnebier, D. A.; Walters, A. J.; Finger, M.; Nafie, L. A.; De Bruin, B.; Buma, W. J.; Woutersen, S. Amplified Vibrational Circular Dichroism as a Probe of Local Biomolecular Structure. *J. Am. Chem. Soc.* **2014**, *136*, 3530–3535.
72. Domingos, S. R.; Hartl, F.; Buma, W. J.; Woutersen, S. Elucidating the Structure of Chiral Molecules by using Amplified Vibrational Circular Dichroism: From Theory to Experimental Realization. *ChemPhysChem* **2015**, *16*, 3363–3373.
73. Tinoco, I.; Freeman, M. P. The optical activity of oriented copper helices: I. experimental. *J. Chem. Phys.* **1957**, *61*, 1196–1200.
74. Feynman, R.; Leighton, R. B.; Sands, M. *The Feynman Lectures on Physics*; Addison-Wesley, 1964.
75. Kumar Pal, S.; Peon, J.; Zewail, A. H. Biological water at the protein surface: Dynamical solvation probed directly with femtosecond resolution Samir. *PNAS* **2002**, *99*, 1763–1768.
76. Peon, J.; Pal, S. K.; Zewail, A. H. Hydration at the surface of the protein Monellin: dynamics with femtosecond resolution. *PNAS USA* **2002**, *99*, 10964–10969.
77. B. Chance, F. The accelerated-flow method for rapid reactions. *J. Inst.* **1940**, *229*, 455–766.
78. Eigen, M.; Norrish, R. G. W.; Porter, G. *Nature* **1949**, *164*, 658.
79. Maiman, T. H. Stimulated Optical Radiation in Ruby. *Nature* **1960**, *187*,

493–494.

80. Hargrove, L. E.; Fork, R. L.; Pollack, M. A. Locking of He-Ne Laser Modes Induced by Synchronous Intracavity Modulation. *Applied Physics Letters* **1964**, *5*, 4–5.
81. Moulton, P. F. Spectroscopic and laser characteristics of Ti:Al2O3. *J. Opt. Soc. Am. B* **1986**, *3*, 125–133.